Structures 86 (2026) 111228

Contents lists available at ScienceDirect

Structures

journal homepage: www.elsevier.com/locate/structures

Identification of soil-structure interaction as the primary source of traffic-induced vibrations in a low-rise building: A nonlinear-elastic perspective

Fabián Consuegra [a,b]

[a] Head of Structural Division, INGETEC, Bogotá, D.C. Colombia
[b] Dept. de Ing. Civil, Universidad Nacional de Colombia Sede Medellín, Medellín, Colombia

ARTICLE INFO

Keywords:
Subject headings: soil-structure interaction
Perceived vibrations
Traffic-induced vibrations
Vibration comfort level of buildings
Nonlinear-elastic SSI

ABSTRACT

Soil-Structure Interaction (SSI) effects may become significant for buildings situated on soft soil when coupled with specific foundation and superstructure flexibility characteristics. Under service conditions, traffic-induced waves can cause vibrations perceptible to building occupants, even when the structure fully complies with a conventional strength-based building standard. This investigation was based on records of a six-story building. Soil foundation was modeled through a semi-infinite elastic media representation. A calibrated model achieved estimations within an 8 % difference from actual field records. The results demonstrate that SSI induces a reduction of up to 40 % in the system's lateral stiffness during its service state at overall drift ratios of about 0.0002 %. In contrast to research approaches focused primarily on inelastic behavior for seismic applications, this study presents a methodology to identify the presence of SSI, by tracking the frequency of an equivalent nonlinear-elastic model. This variation occurs as base movement activates foundation flexibility, leading to the coexistence of two distinct fundamental frequencies. The identification is achieved through a 2-DOF representation and it involves (a) analyzing the frequency content of ambient vibrations recorded with high-sensitivity instrumentation; (b) tracking the fundamental frequency as a function of displacement; (c) establishing a linear transfer function (TF) to isolate the effects of soil flexibility; and (d) comparing estimated forces applied at each DOF to localize the source of energy input. The method was successfully implemented to characterize the most probable scenario causing user-perceived vibrations. Despite its efficacy, the applicability of this approach may be limited in cases with low signal-to-noise ratios or highly rigid superstructures that preclude the coexistence of the fixed-base and SSI-influenced frequencies.

1. Introduction

Vibration control is generally not a primary design parameter for buildings according to structural design standards [1,2], unlike for other structure types such as pedestrian bridges [3]. For the latter, adequate strength and stress limits must be met, but the structure must also satisfy specific rigidity requirements to ensure the natural frequency of the bridge does not fall within the range of frequencies perceptible to humans. Furthermore, the bridge's frequency must remain sufficiently distant from human walking excitation frequencies to avoid resonance that causes discomfort and a sense of unsafety for users.

While extensive literature recommends vibration control—including for local vertical vibrations in steel systems [4] and other recommendations lacking strict enforcement in structural design [5] —there is a noticeable lack of official standards prescribing vibration control for lateral displacements in buildings as part of structural or geotechnical design. This deficit exists despite the long-recognized relevance of lateral Soil-Structure Interaction (SSI) in seismic applications [6] [7]. For tall buildings, aerodynamic studies, such as wind-tunnel analysis, are often performed during the structural design phase to prevent user discomfort under service conditions. However, some recommendations that prescribe controlling service vibrations in the structure neglect to include the foundation in the analysis [8], even though the effect of foundation flexibility on service vibrations is a recognized factor [9,10].

For low-rise buildings, vibration control is rarely addressed, taking precedence over seismic analysis in current standards [1,2]. From a simplified perspective, a building may be conceived as a 2-DOF system, with one degree of freedom of lateral displacement assigned to the

E-mail address: fabianconsuegra@ingetec.com.co.

https://doi.org/10.1016/j.istruc.2026.111228
Received 23 October 2025; Received in revised form 30 December 2025; Accepted 27 January 2026

superstructure and one to the foundation, based on the assumption of negligible rocking over deep foundations during service conditions [11] (in contrast to seismic practice). SSI is typically addressed in design standards only for extreme or unusual conditions like earthquakes [12–14], primarily to achieve a more accurate estimation of the structural natural period used to calculate seismic forces. For routine design purposes, structural engineers often assume fixed-base conditions, neglecting flexibility derived from soil properties. Consequently, SSI is often disregarded, despite the lack of consensus regarding the conservatism of this assumption [15,16]. Although neglecting SSI may be justifiable from a seismic design perspective (as a stiffer building attracts greater seismic forces), this approach is not always conservative regarding displacement or flexibility related to user comfort.

This paper investigates a six-story building that meets strength code requirements but experienced perceived vibrations by users under normal-day conditions. The study employs a method combining analytical models with actual vibration records to assess the complex interaction between the environment, foundation, and superstructure, leading to the conclusion that Soil-Structure Interaction is the main source for the perceived vibrations. In complementing existing research, novel perspective of the presented methodology to identify SSI and estimate its effect in the perceived in-service condition vibrations, might be defined by the combination of the following essential aspects:

- Usage of a simplified 2-DOF representation in numerical model as well as in data recording
- Selection of adequate instrumentation capabilities to observe SSI at small amplitudes
- identifying how foundation flexibility contributes to both an increase in overall system flexibility and the introduction of base movements that are subsequently amplified at higher stories. This identification is performed by analyzing standard Fourier Amplitude Spectra, tracking the variation of the fundamental frequency at low displacement levels, calculating linear-elastic Transfer Functions to isolate the effects of soil flexibility, and estimating the forces applied at each degree-of-freedom (DOF) within the system.

A novel aspect of this research lies in the identification of a dual-spectral signature within the building's dynamic response, characterized by the coexistence of two distinct fundamental frequencies depending on the excitation level, thus, a behavior represented in this study by a nonlinear-elastic model. While traditional Soil-Structure Interaction (SSI) studies, such as the landmark analytical frameworks by Veletsos and Meek [6] and the empirical observations by Stewart et al. [17], typically treat the system as having a singular shifted frequency (f), the presented field data reveals a transitionary behavior. Moreover, many recent research continues to focus on the effect of SSI for seismic applications where an inelastic model is used [18–22] rather than a nonlinear-elastic model. At ultra-low ambient noise levels, the system studied exhibits a peak at 3.02 Hz, corresponding to a 'quasi--fixed' base condition where foundation flexibility remains immobilized. However, during transient traffic events, a secondary dominant peak emerges at 2.53 Hz. This elastic frequency coexistence serves as a reference method for SSI identification, providing a direct empirical measure of the 40 % reduction in lateral stiffness without the uncertainties inherent in purely numerical or laboratory-based soil stiffness estimations. This transitionary elastic non-linearity bridges the gap between theoretical fixed-base models and the actual service-level performance of buildings on soft soil.

2. Case study

This section describes the building used for the current research in terms of geometric configuration and material and relevant structural and geotechnical properties for the superstructure and foundation. Also, selected instrumentation and signal records obtained, are discussed to illustrate how required accuracy was provided for such small displacements. The investigated structure is a six-story reinforced concrete (RC) building comprising four stories of superstructure above grade and two underground parking levels, as shown in Fig. 1.

The lateral force-resisting system consists of moment-resisting frames in both horizontal directions. Inter-story heights are 4.5 m for the first level and 3.5 m for the subsequent levels. Column dimensions vary from 30 cm× 70 cm at the upper levels to 40 cm× 100 cm at the lower levels. The strong direction of most columns is aligned with the short in-plan direction (y-direction). The foundation system is a piled-raft foundation consisting of 126 floating piles, each 25 m long and 40 cm in diameter. The specified design concrete strength (f′c) was 21 MPa for beams and columns and 24 MPa for other elements The building features an L-shape in plan, with the longest dimension of the foundation (x-direction) measuring between 1.5 and 2.3 times the length of the short dimension (y-direction). The foundation extends beyond the superstructure, being 9 m wider and 3 m longer in plan. Based on soil exploration data, seismic micro-zonation studies [23], and local structural standards [2] of similar international classification [1–24], the soil profile is classified as Type S4, characterized by an average shear wave velocity (v_s) of 150 m/s. Material samples extracted to a depth of 12 m were classified as either CH or MH according to the Unified Soil Classification System (USCS) [25]. The instrumentation was selected of microtremors accelerometers (0.5 g-full range) combined with high resolution acquisition system (24-bits), such that a theoretical resolution of the system of 5×10^{-5} milllig was achieved. However, actual measurements were used to verify the more relevant characteristic of signal-to-noise ratio (SNR) that dictates accuracy of records [26]. Based on measurements of surrounding ground (superstructure records are a few orders of magnitude larger and then much less prone to be overcome by noise level), the average SNR were obtained between 2 and more than 5, which is considered adequate for experimental studies [26].

The building occupants reported experiencing perceptible vibrations during normal-day conditions on the fourth floor, specifically near the southwest corner of the building, a location which corresponds to the point farthest from the in-plan center of rigidity. The highest volume of traffic near the building is on a busy street aligned with the building's long-plan dimension. The experimental phase included the following components: a) Ambient vibration records captured in the vertical and the two main horizontal directions; b) Vibration records obtained during the passage of a heavy vehicle around the building while extraneous traffic was restricted; c) Simultaneous floor vibration records taken across the structure in the main horizontal directions; d) Vibration records acquired in the soil surrounding the foundation.

3. Numerical model

This section provides a detailed description of the two versions of a 3D model used for analysis and interpretation of records. A third model based on a 2-DOF representation, essential to the simplified method presented, shall be presented in Section 5. A three-dimensional Finite Element (FE) model [27] was developed based on the as-built structural drawings for the superstructure, comprising almost 13,000 degrees of freedom (Fig. 2). The model utilized frame elements for beams and columns and shell elements for the slab representation. The modulus of elasticity of concrete (E_c) was estimated using the formula $E_c = 4700\sqrt{f'c}$ (MPa) [2], which is equivalent to the ACI [1], with the concrete strength assumed to be 20 % higher than the design value based on expected hardening over more than a decade post-construction. Non-structural elements, such as masonry walls in the stair cores, were included in the model due to the observed strong sensitivity of the calculated natural frequencies to their presence. Constrained conditions were imposed on the slab nodes representing the perimeter of the columns on each floor to accurately model the slab-column connections.

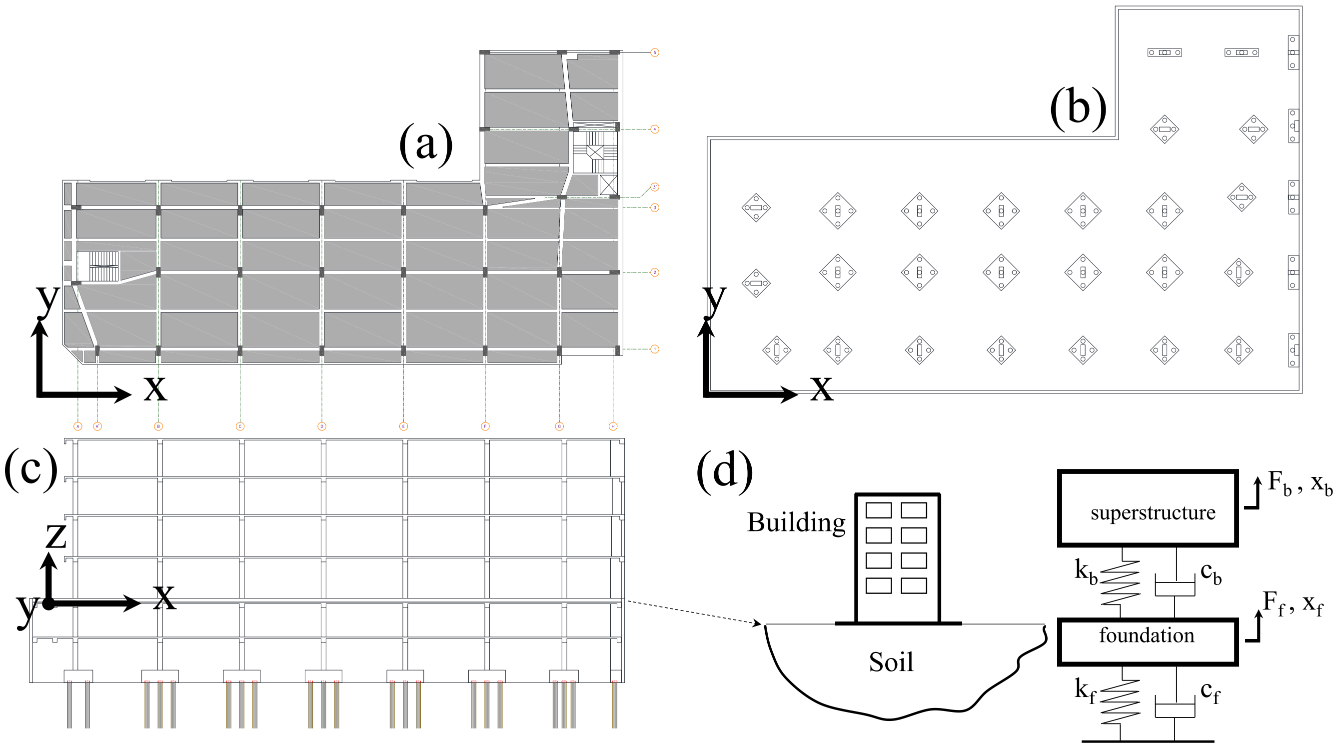

Fig. 1. Building description, coordinate system and 2-SDOF system: (a) typical floor-plan view; (b) foundation plan view surrounded by walls; (c) elevation showing superstructure, underground floors and foundation, and (d) 2-DOF model to represent the system.

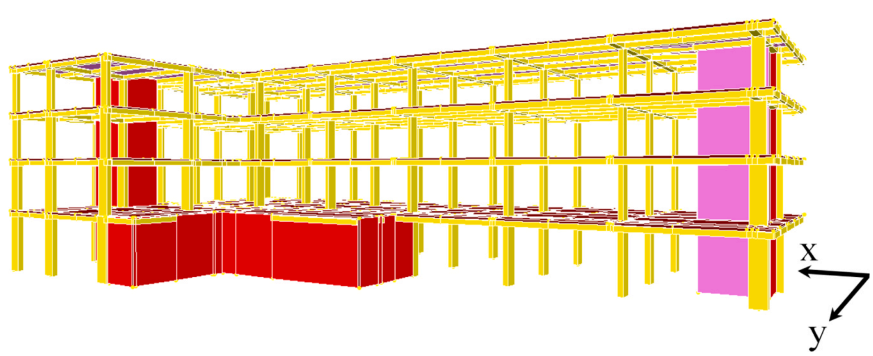

Fig. 2. Three-dimensional Finite Element Model used: the superstructure is fully represented in geometry (frame elements for beams and columns and shell elements for walls) while foundation was represented by stiffness, damping and mass properties concentrated at base of columns. Coordinate system used is presented.

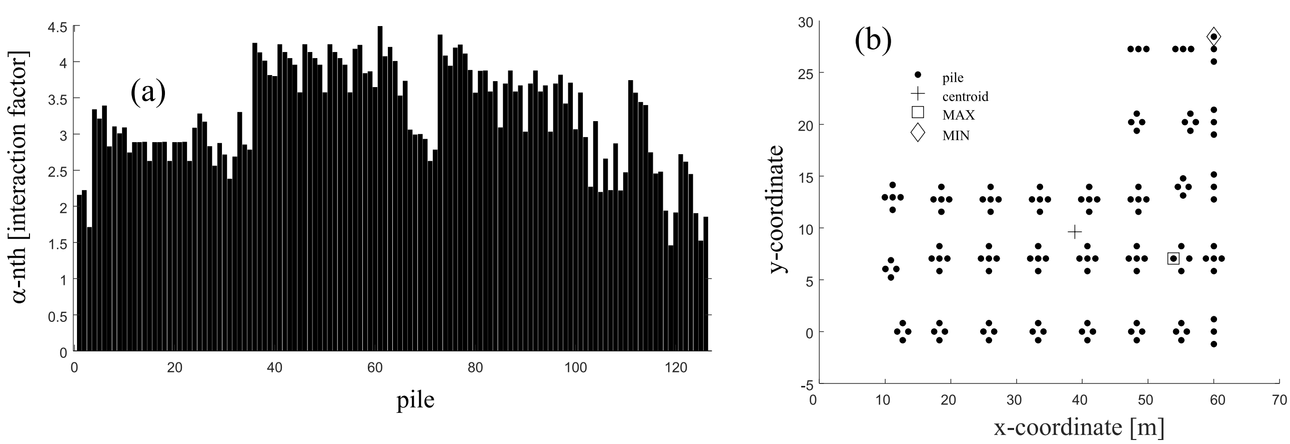

Fig. 3. Pile interaction factor α-th used to represent foundation flexibility, computed for X-direction: (a) value obtained for each pile based on over 7800 combinations; (b) Pile layout showing specific piles with maximum and minimum interaction values.

The foundation system's dynamic stiffness was represented in the numerical model using a semi-infinite elastic media consideration, as proposed by Novak [28] [29], utilizing soil and concrete pile properties (Fig. 3). To account for the flexibility induced by pile proximity, the interaction factor a (an-th) between the n-th pair of piles out of the total of 126 piles, was calculated along the two main horizontal directions [30]. This analysis considered over 7800 combinations of pile pairs for each in-plan direction [31]. The lateral pile stiffness, k, was calculated assuming a head-rotation restrained condition—provided by the foundation mattress footing, as $E_pI_p/{r_o}^3 * f_{11,1}$, where the coefficient $f_{11,1}$ is a frequency-dependent parameter. These expressions were derived as a function of the pile flexibility factor, $K_R = E_pI_p/GL^4$, which depends on the pile's modulus of elasticity (E_p), pile moment of inertia (I_p), pile radius (r_o), the soil shear modulus (G), and the pile length (L). An illustration of this procedure, specifically the estimated α value for each pile and the piles exhibiting maximum and minimum interaction in the x-direction, are shown in Figs. 3(a) and 3(b).

Consistent with concentrating the foundation stiffness at the column bases at the ground level, the total mass of the two underground parking levels was equally distributed among the column base nodes in the FE model (Fig. 2). This simplification was justified because the basement levels possess the stiffest columns and benefit from substantial lateral stiffness provided by the perimeter retaining walls, making distortion across the foundation during service vibrations negligible. The stiffness of these walls is, in fact, two orders of magnitude larger than that of the columns alone. The model's validity was later justified by comparison with actual records. A detailed list of parameters used in the numerical modeling, based on two scenarios of soil flexibility (shear wave velocities of 150 m/s and 133 m/s), is provided in Table 2. The resultant numerical models demonstrated a maximum average difference of only 8 % when compared to actual measurements (as labeled "error" in Table 1), confirming the reasonability of the models obtained.

4. Dynamic Behavior of Building

This section presents the comparison between analytical results of the numerical models (3D model in its two versions and a 2-DOF model) and actual records, in order to show both the fundamental-frequency coexisting effect and amplification of traffic waves in the building, due to SSI.

Table 1
Main natural frequencies calculated and identified.

Parameter/quantity	Value (s)*			unit
Foundation stiffness, k_f	2876	/	2491	kN/mm
Average interaction factor for x and y directions	1.629	/	1.644	rad
Pile flexibility factor, K_R by Poulos			3.01*10^-6	rad
Shear wave velocity	150	/	133	m/s
Foundation lateral-stiffness coefficient by Novak, $f_{11,1}$	0.040	/	0.034	rad
Foundation damping, c_x			0.477	MN*s/m
Equivalent superstructure SDOF mass, m_b	1777,335	/	1718,834	kg
building-to-foundation frequency ratio, η	0.693	/	0.583	rad
building-to-foundation mass ratio, μ	0.535	/	0.517	rad
Foundation viscous damping ratio, ζ_f			1.2 %	rad
Superstructure viscous damping ratio, ζ_b			0.7 %	rad
Foundation and superstructure 1st-mode energy deformation	4.653*10^3	/	1.509*10^3	Joule/m^2
SDOF-system viscous damping ratio, ζ			0.83 %	rad

4.1. Ambient vibration tests

The main mode shapes for the two horizontal directions x and y calculated with the FE model are shown in Fig. 4, where shaded images representing undeformed position are to help on visualizing the deformed shapes. The Fig. 4(a) thru (d) correspond to in-plan and elevation deformed shapes for the first mode of each direction, whereas Fig. 4(e) and (f) correspond to elevation deformed shape of second modes.

It can be seen that despite direction, first and second modes are deformed shapes where superstructure is in and out of phase with respect to foundation (columns base) respectively, as expected for a 2-DOF system. These two modes account for a significant portion of the total response, summing up between 70 % and 80 % of the total participating mass (MM) calculated for each direction, as seen in Table 1. The first mode shape for the x-direction contains a notable component of displacement in the y-direction as the non-symmetric configuration of the building induces rotation around center of rigidity. This asymmetry dictates that the maximum y-direction displacements for the first x-direction mode occurs at the building's left corner of plan view in Fig. 1(a), the reported location of perceived vibrations at the highest floor level, as estimated also with the model shown in Fig. 4 (b).

Table 1 provides a comparison of the calculated natural frequencies from the FE model against the experimental records, alongside the computed Modal Mass (MM) for the two primary modes in each direction. Fig. 5(a) and Fig. 5(d) present the Fourier Spectrum Amplitude (FSA) derived from acceleration records corresponding to one-hour and two-minute time windows, respectively. The comparison of fundamental frequencies between these two spectra illustrates how observation may be distorted by accumulated noise level as a longer time-window record is considered. Thus, frequencies $f_{1\text{-}y}$ and $f_{1\text{-}y\text{-fixed}}$ seem more distinguishable in the short-duration spectrum (Fig. 5d) than at the long one (Fig. 5a), therefore aspects such as the SNR described in Section 4 need to be considered. The spectra displayed in Fig. 5(b) (at the center of the floor slab) and Fig. 5(c) (at the right edge) were recorded simultaneously with the record shown in Fig. 5(a). The maximum recorded acceleration during the ambient vibration test, observed within the target frequency range of 0.5 Hz to 8 Hz, measured 0. 2 millig (2 10^{-4} g). The fundamental natural frequencies of the building were identified from the peak amplitudes of these spectra: $f_{1\text{-}x} = 2.06$ Hz and $f_{1\text{-}y} = 2.53$ Hz (summarized in Table 1).

Fig. 5(e) summarizes a series of tests where sensors were positioned along a straight path between axes A and H of Fig. 1(a). The mode shape was determined from these tests using the phase angle in the frequency domain between signals obtained from adjacent sensors [32,33]. Fig. 5 (e) experimentally confirms the main mode shape derived from the FE model (Fig. 4b). Crucially, the location of the maximum displacement point determined from this test is consistent with the area of most significant/disturbing vibrations reported by occupants at the left boundary of the building floor. The second natural frequency in the y-direction ($f_{2\text{-}y}$) is clearly observed at 5.15 Hz in Figs. 5(a) through 5(c) (as summarized in Table 1). The peak amplitudes (Fourier amplitudes) corresponding to this frequency ($f_{2\text{-}y}$) are notably similar across simultaneous records at the left, center, and right boundary positions, which is consistent with the mode shape calculated by the FE model (Figs. 4d and 4f) that suggests a nearly uniform y-lateral floor movement. Quantitatively, when comparing the peak magnitudes in the Fourier Spectra (Fig. 5a–c), the second frequency ($f_{2\text{-}y}$) contributes between 10 % and 20 % of the energy observed at the fundamental frequency ($f_{1\text{-}y}$) across the left and center floor slab locations, which collectively encompass nearly 70 % of the total plan area. The calculated modal mass (MM) for the second fundamental frequency ($f_{2\text{-}y}$) is approximately half the MM of the first mode ($f_{1\text{-}y}$) (as documented in Table 1), a relationship that remains consistent regardless of the assumed soil stiffness scenario (defined by the shear-wave velocities). This analytical finding is

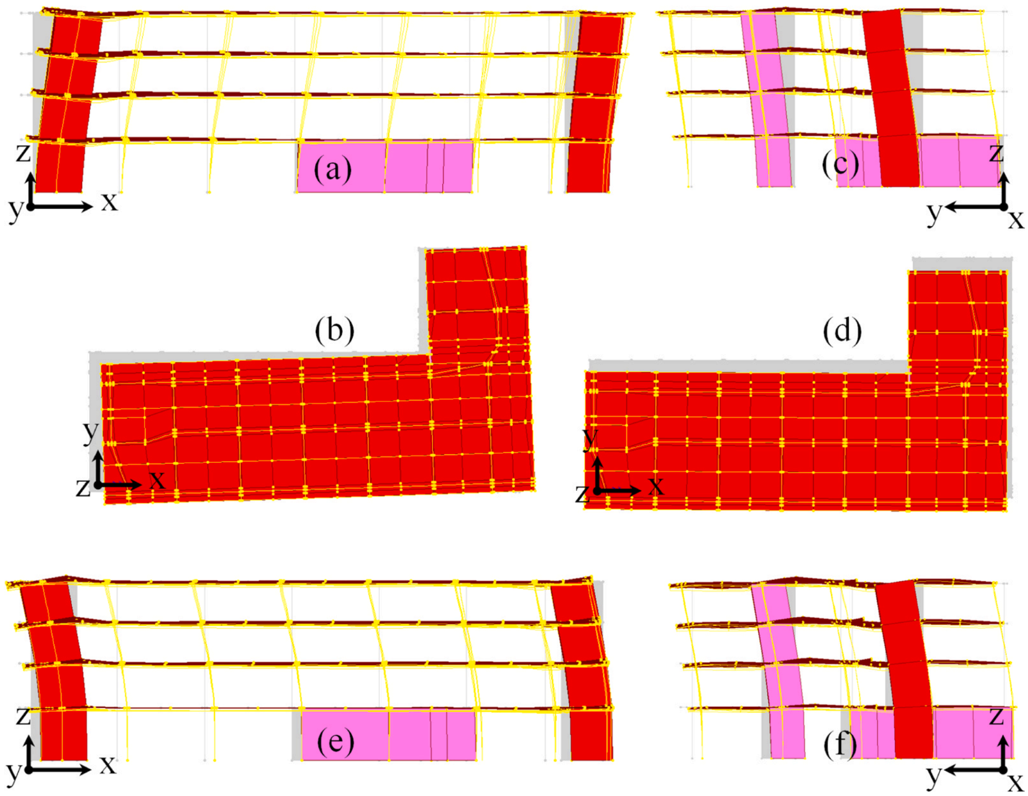

Fig. 4. Main mode shapes views calculated with the 3D model: (a) and (b) elevation and plan view of 1st mode shape of x-direction; (c) and (d) elevation and plan view of 1st mode shape of y-direction; (e) elevation of 2nd mode shape for x-direction; (f) elevation of 2nd mode shape for y-direction.

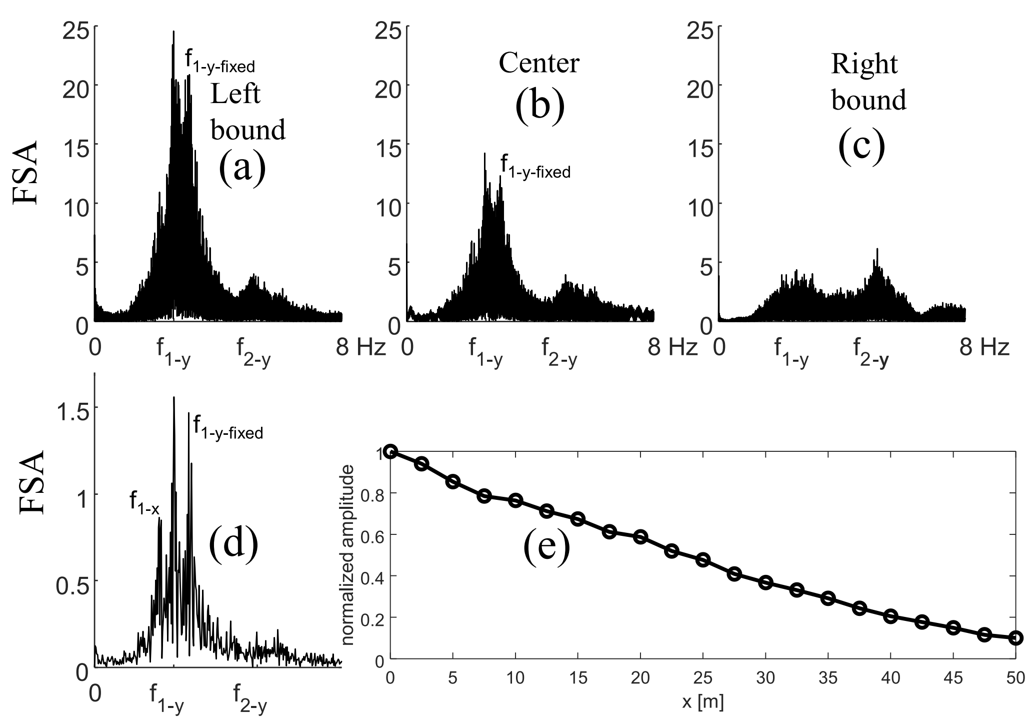

Fig. 5. Ambient vibration records measured along y-direction: (a), (b) and (c) are Fourier Spectra Amplitudes of 1-hour ambient vibrations measured at left, center and right bound of building plan at 4-th floor, respectively; (d) Fourier Spectrum Amplitude of 1-minute ambient vibrations measured at left bound; (e) amplitude-normalized accelerations measured along an x-direction straight path between axes A and H of Fig. 1(a).

supported empirically by the average ratio of peak amplitudes observed in the spectra across Figs. 5(a) through 5(c). Furthermore, close inspection of the spectra (Fig. 5a–d) reveals that each identified frequency corresponds to a spread-over energy distribution rather than the sharp, crystalline peak characteristic of a perfectly linear-elastic system. This spectral spreading suggests the presence of some degree of non-linear elastic behavior within the structural concrete [34–37].

Consistent with the structure's non-symmetric deformation pattern predicted by the numerical model (Fig. 4b), the longitudinal frequency, $f_{1\text{-}x}$, exhibits a noticeable presence within the transverse (y-direction) spectrum. The observed relationship between these two fundamental frequencies is consistent with the column orientation, resulting in $f_{1\text{-}y}$ being greater than $f_{1\text{-}x}$. Further spectral analysis reveals a distinct peak corresponding to the fixed-base natural frequency in the y-direction $f_{1\text{-}y\text{-}fixed}$ at 3.02 Hz. This peak, evident in Fig. 5(a), (b), and (d), represents the vibration of the superstructure at very small amplitudes before the foundation's flexibility is fully mobilized as will be shown. Thus, below certain displacement levels of the foundation and from a practical perspective, the building superstructure behaves as fully restrained at the base of its columns and no noticeable SSI is observed (no relevant movement of the foundation itself). Therefore, the system behaves as a nonlinear-elastic system if no permanent displacement is caused [37], as expected for small strain levels proper of the service condition.

4.2. Coexisting fundamental frequencies

The two distinct y-direction fundamental frequencies, representing the behavior with SSI ($f_{1\text{-}y}$) and the theoretical fixed-base condition ($f_{1\text{-}y\text{-}fixed}$), are visually observable in the center plot (middle portion) of Fig. 6 (c). This plot displays the Fourier Amplitude Spectrum (FSA) of the 4-th floor acceleration record captured during the passage of a heavy vehicle. It is important to note, related with the nonlinear behavior described, that this vehicle test imposes larger displacement in the system than those displacements corresponding to ambient vibration of Fig. 5. Specifically, the amplitudes in Fig. 6 (truck event) are approximately 0.8 millig (8×10^{-4} g), compared to the 0.2 millig (2×10^{-4} g) measured in the ambient records (Fig. 5). It is evident in this spectrum of Fig. 6(c) that the contribution of $f_{1\text{-}y\text{-}fixed}$—a peak identified through the transfer function derived separately as will be explained in Section 5—appears significantly less dominant under the relatively larger vibration amplitudes imposed by the passing truck (peak magnitude in the FSA for $f_{1\text{-}y}$ is larger than peak for $f_{1\text{-}y\text{-}fixed}$).

The comparison of the two fundamental y-direction frequencies ($f_{1\text{-}y}$ and $f_{1\text{-}y\text{-}fixed}$) in Figs. 5 and 6 leads to a critical observation: at small amplitudes, when the foundation's flexibility has not yet been mobilized, the superstructure behaves as if supported on a fixed foundation ($f_{1\text{-}y\text{-}fixed}$). Conversely, when vibration amplitudes are large enough to enforce foundation movement, the system transitions to exhibiting the characteristic SSI-vibrating behavior associated with $f_{1\text{-}y}$. This dual-spectral condition or coexisting fundamental-frequency condition, has been further analyzed via a spectrogram calculated on the 4-th floor response of the passing-truck test and shown at the top of Fig. 6(a). The spectrogram shown [31] corresponds to successive time-windowed Fourier transformations over the total record duration, in order to evaluate frequency content of the response over time. It is seen in this spectrogram that as the vibration amplitude decreases a higher frequency is revealed in the contour, for instance, right after vehicle arrival ($t_{arrival}$) the colored zone in the spectrogram shifts down in the frequency vertical axis. Estimates in this type of plot are subjected to the natural trade-off between time and frequency precision [38], therefore a spread-energy contour is being observed in the spectrogram of Fig. 6(a) rather than a sharp frequency value for each instant of the record.

In order to complement the observation of the displacement-dependency of the frequency in the spectrogram of Fig. 6(a), an additional estimate of fundamental frequency has been performed based on the concept of instantaneous frequency [39], that led to calculate a vibrating frequency at each instant of the record rather than within a time window as the spectrogram technique. Equations 1 (a), (b) and (c) were used to estimate the instantaneous *f(t)* of the 4-th floor response under the passing-vehicle test of Fig. 6. A narrowed band-passed filter was used to isolate the frequency content of the response between a 1 and 4 Hz corresponding to a range that contains the two fundamental frequencies previously identified as the dual-spectra effect ($f_{1\text{-}y}$ and $f_{1\text{-}y\text{-}fixed}$). Figs. 7(a) and 7(b) show the time and frequency-domain of the filtered signals (ground and 4-th floor responses of experiment in Fig. 6), which are almost identical to those shown in Fig. 6(a) given that passing-vehicle response is dominated by the fundamental frequency. It can be seen in the spectra of Fig. 7(b) that the fixed-fundamental frequency ($f_{1\text{-}y\text{-}fixed}$), thus, under no SSI effect, is more evident at the superstructure response than at the ground response given that foundation has negligible movement at such frequency, or, in other words, foundation flexibility has not been engaged yet at smaller displacments.

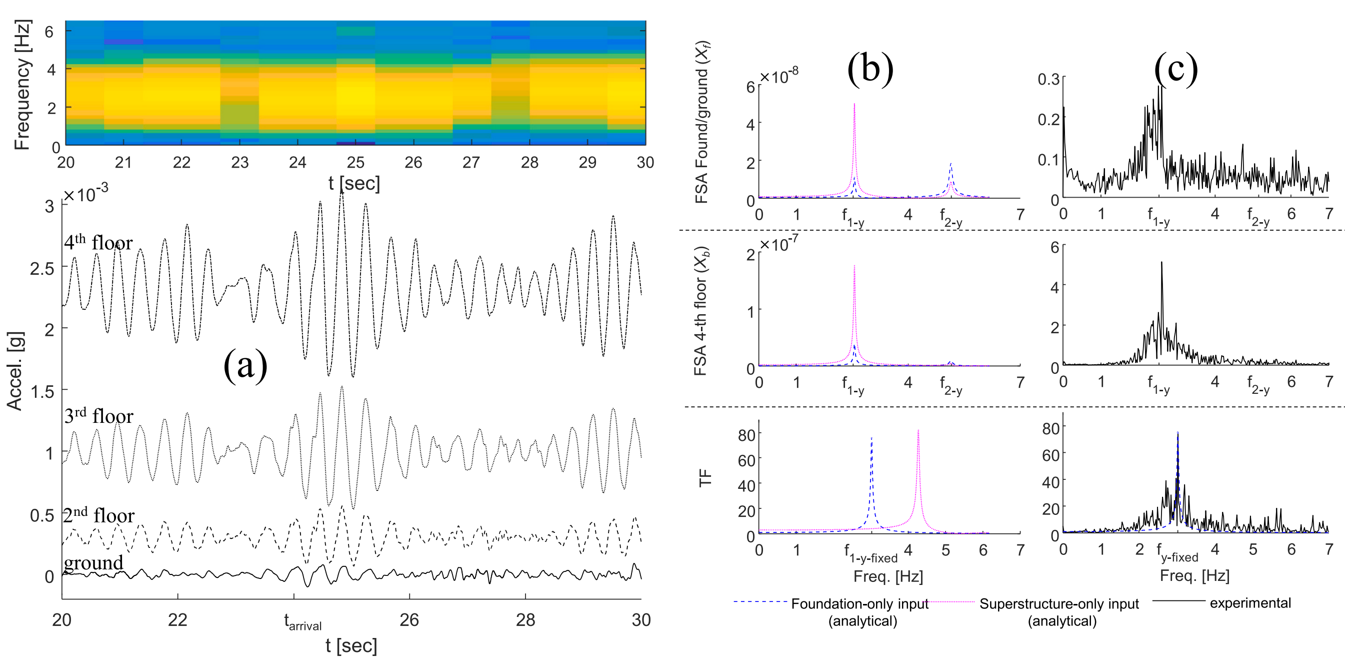

Fig. 6. Passing truck testing in the building measured along y-direction: (a) acceleration records at ground and superstructure floors and spectrogram of 4-th floor; (b) Analytical response of a 2-DOF representation, with Fourier Spectrum Amplitudes for foundation (top plot) and superstructure (mid-plot) and the corresponding Transfer Function between foundation and superstructure (bottom plot); (c) The same results of the three plots in (b) obtained experimentally.

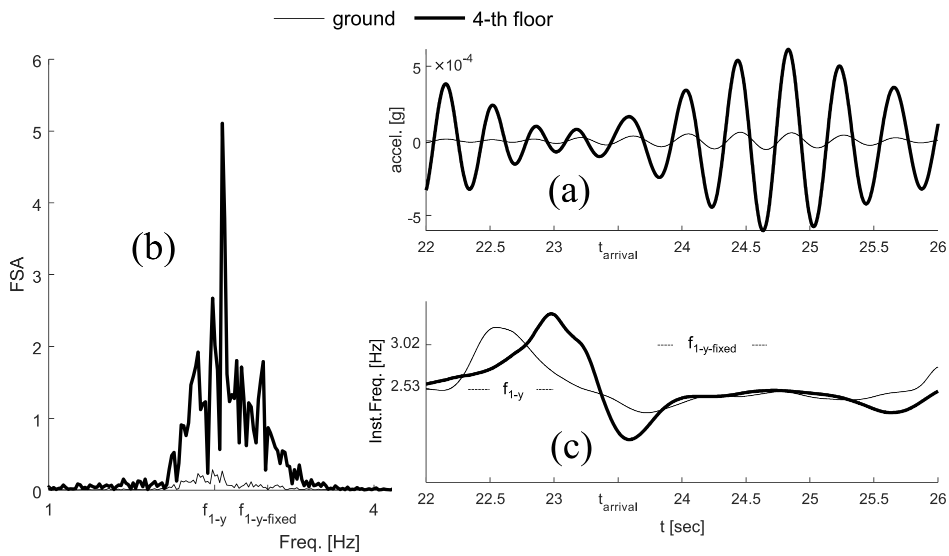

Fig. 7. Tracking fundamental-frequency variation of y-direction: (a) Isolated fundamental frequency response via EMD processing; (b) FSA of isolated ground and superstructure responses; (c) Instantaneous Frequency calculated via Hilbert Transform.

Fig. 7(c) shows the instantaneous frequency calculated for a time window around vehicle arrival instant ($t_{arrival}$) as marked in Fig. 6(a). Consistent with the dual-spectra phenomenon of presence of two fundamental frequencies in the building system, it can be seen in Fig. 7 (c) that for very little movement in the superstructure just before vehicle arrival, the superstructure vibrates according to the fixed-fundamental frequency ($f_{1\text{-}y\text{-}fixed}$) and once acceleration amplitude (and also displacement) of the building system is increased by the vehicle effect, the instantaneous frequency drops to a value about the SSI fundamental frequency ($f_{1\text{-}y}$) indicated in Table 1. Also, after the temporary vehicle effect has passed near the end of the time window, the instantaneous frequency tends to return to higher values associated to no foundation movement. This is the coexisting fundamental-frequency phenomenon mentioned, which can be visualized from the perspective of a non-linear elastic system as previously illustrated in the spectrogram of Fig. 6(a).

$$x'(t) = \int_{-\infty}^{\infty} \frac{x(u)}{\pi(t-u)} du \tag{1a}$$

$$X(t) = x(t) + ix'(t) = A(t)e^{i\theta(t)\cdot t} \tag{1b}$$

$$f(t) = \left(\frac{1}{2\pi}\right)\frac{d\theta(t)}{dt} \tag{1c}$$

5. Identification of soil flexibility under passing-truck testing

This section presents a comparison of the proposed analytical 2-DOF modeling and actual records to identify mobilization of the foundation flexibility under realistic passing-truck tests. A dedicated series of controlled field tests were executed by restricting regular traffic and exclusively passing a 17-tonf vehicle around the structure. An accelerometer was strategically placed near column 3 A on each floor (the location where vibrations were consistently reported). For each test run, the sensors, installed at the ground, second, third, and fourth floor levels, were precisely aligned along either the x or y principal direction. Continuous radio communication was maintained with the truck driver during testing to accurately pinpoint the precise moment the vehicle passed in front of the building at a near-constant speed of 40 kph. The vehicle's key characteristics (weight, path, and speed) were carefully chosen to closely match the parameters of the prevalent daily traffic conditions around the site. Fig. 6(a) presents the acceleration records along the y-direction, spanning from the ground level to the top floor. The moment the vehicle arrived (at approximately 24 s), all sensors simultaneously registered a sharp increase in acceleration. The maximum amplitude reached 0.0008 g (0.8 millig) at the fourth floor. The records across the floors consistently reveal that the primary structural response is controlled by the first mode shape, where all levels move coherently (in-phase) toward the same direction at any given instant, with displacements progressively amplifying toward the upper floors, consistent with similar findings in structural response studies for SSI [40] [41].

Consider a 2-DOF system representation with lateral displacement at foundation x_f and superstructure x_b as shown in Fig. 1(d) and as described in Table 1. The dynamic equilibrium can be written as that in Eq. 2(a) in the time domain where M, C and K represent respectively mass, damping and stiffness matrices, and superposed dots represents time derivatives. To transition Eq. 2(a) from time to frequency domain, each time-dependent variable and the forcing function can be represented in harmonic form: $x_f = X_f e^{i\Omega t}$, $x_b = X_b e^{i\Omega t}$ and $F = F_o e^{i\Omega t}$. The frequency-domain representation of the 2-DOF system [42] is provided by Eq. 2(b) where X_f and X_b represent the Fourier Transform of displacements, $i = \sqrt{-1}$ and $\Omega = 2\pi f$ is the forcing frequency [rad/s] with f expressed in Hz. If the forcing function is selected as $F_o = \begin{Bmatrix} 1 \\ 0 \end{Bmatrix}$, it defines an assumption of foundation-only input, representing a unit force applied solely at the foundation DOF. This simulates the entry point of potential traffic-generated waves into the coupled foundation-superstructure system, with no direct force applied to the superstructure.

$$[M]\begin{Bmatrix} \ddot{x}_f \\ \ddot{x}_b \end{Bmatrix} + [C]\begin{Bmatrix} \dot{x}_f \\ \dot{x}_b \end{Bmatrix} + [K]\begin{Bmatrix} x_f \\ x_b \end{Bmatrix} = \begin{Bmatrix} F_f \\ F_b \end{Bmatrix} \tag{2a}$$

$$\left[\ -[M]\Omega^2 + [C]i\Omega + [K]\ \right]\begin{Bmatrix} X_f(\Omega) \\ X_b(\Omega) \end{Bmatrix} = \begin{Bmatrix} 1 \\ 0 \end{Bmatrix} \tag{2b}$$

Fig. 6(b) displays the analytical displacement responses for the foundation (X_f) and the superstructure (X_b), calculated using Eq. 2(b) with the foundation-only input assumption. The plot located at the bottom of Fig. 6(b) presents the Transfer Function (TF), which is derived as the ratio of these two frequency-domain responses, thus, $TF = X_b/X_f$. Additionally, Fig. 6(b) includes a second set of analytical results corresponding to the superstructure-only input. This scenario utilized a forcing function vector set to $F_o = \begin{Bmatrix} 0 \\ 1 \end{Bmatrix}$. For both sets of analytical functions, the damping matrix C was defined using Rayleigh proportional damping [36], ensuring that the equivalent damping ratio for a given mode matches the energy-weighted values established for the complete foundation-superstructure system (Table 2).

Although these previous analytical expressions (equation 2) represent displacement components transformed into the frequency domain, their Transfer Function (TF) ratio remains valid for either displacements or accelerations (measurements consist of accelerations). The peaks observed in the Fourier Spectrum Amplitude (FSA) derived from the analytical signals (Fig. 6b), specifically at the foundation (ground) and superstructure (4-th floor), align precisely with the two natural frequencies of the SSI system, $f_{1\text{-}y}$ and $f_{2\text{-}y}$. In general terms, the peaks evident in the FSA of foundation and superstructure (the top two plots of Fig. 6b) are precisely located at the two natural frequencies of the full SSI-system, $f_{1\text{-}y}$ and $f_{2\text{-}y}$, as expected.

Crucially, the largest peak for both the foundation (ground) and the superstructure (4-th floor) occurs at the first fundamental frequency ($f_{1\text{-}y}$). Conversely, each Transfer Function (TF) shown in the bottom plot of Fig. 6(b) exhibits a unique peak. In the case of the foundation-only input TF, this peak analytically corresponds to the theoretical fixed-base structural condition, simulating a scenario where no SSI is present (i.e., a rigid foundation) [43] [44]. Analogously, the unique peak observed when using the superstructure-only input TF corresponds to the isolated foundation frequency as if no superstructure were present (which can be verified using the mass and stiffness parameters in Table 2). Fig. 6(c) presents the same analytical results structure but incorporates actual field records taken from Fig. 6(a). Middle plot of Fig. 6(c) was used previously to illustrate the existence of the two fundamental frequencies $f_{1\text{-}y}$ and $f_{1\text{-}y\text{-fixed}}$, associated to the nonlinear behavior of the system with displacement amplitude. The bottom plot of Fig. 6(c) specifically compares the experimental TF with the analytical TF generated using the foundation-only input (taken from the bottom plot of Fig. 6b). This comparison enabled the identification of the building's fixed-base natural frequency as $f_{1\text{-}y\text{-fixed}} = 3.02$ Hz (Table 1). Furthermore, this information confirms that the structure does not behave under a rigid-foundation assumption, even during low-amplitude service vibrations. Based on the fundamental frequencies observed for the fixed (3.02 Hz) versus the SSI (2.53 Hz) condition (Table 1), a stiffness reduction of approximately 40 % is estimated due to the presence of Soil-Structure Interaction (SSI). Although soil flexibility reduces the system frequency by a minor proportion compared to what has been observed in larger displacement scenarios typical of earthquakes [11], this proportion plays an important role in the perceived vibrations during service conditions. The magnitude of the TF is exclusive function of damping of superstructure $|TF| = 1/2\xi_b$. The maximum value of the TF represents the condition of resonance, occurring when the excitation frequency equals the natural frequency. With an estimated value of $\xi_b = 0.7\%$, this suggests a potential amplification factor of about 70 if steady-state condition were to be achieved. Crucially, while this maximum amplification factor does not directly depend on the soil, it is the soil-foundation flexibility that allows the traffic waves to transform into an effective input force (F_f in Fig. 1d). The actual, realized amplification will approach this maximum value as closely as the input frequency associated with the soil stratum characteristics ($T_{soil} = 4\ h/v_s$) falls within the vicinity of the system's SSI-frequency.

Fig. 8 illustrates the measured ground vibrations in the y-direction obtained from the soil surrounding the foundation, captured at a horizontal distance of 1 m from the foundation perimeter (bottom boundary in Fig. 1b). Ambient vibration records were collected across three designated zones—left, center (near the building's midportion), and right boundary—consistent with the convention used for the superstructure measurements in Fig. 5. Figs. 8(a) through 8(c) present the acceleration records in the time domain, while their corresponding Power Spectral Densities (PSD) are shown in Figs. 8(d) through 8(f). In these spectra, the main lateral frequencies of the building $f_{1\text{-}x}$, $f_{1\text{-}y}$, $f_{2\text{-}x}$, and $f_{2\text{-}y}$) are clearly marked along the horizontal axes. The values plotted on the vertical axes of the PSD plots were normalized using the factor "2 N" [26] [39] (related to the sampling size) to ensure a meaningful comparison across different time windows. The alignment of the building's natural frequencies with the largest spectral peaks demonstrates that the soil-building vibration is influencing the surrounding ground, as is characteristic of a system undergoing SSI. Furthermore, Fig. 8 reveals that the ground vibrations are significantly larger at the left boundary compared to the right boundary. This asymmetry in the ground response is consistent with the mode shapes of the building that exhibit noticeable in-plane torsional movement. Consistently with this observation, the root-mean-square (RMS) values for the acceleration records measured at the left, center, and right boundaries were 0.9 millig, 0.4 millig, and 0.6 millig, respectively. These values resemble the controlling influence of the first mode ($f_{1\text{-}y}$), which produces larger movements at the extreme boundaries of the building, with the largest magnitudes occurring at the left boundary where vibrations were reported. According to the spectrum presented in Fig. 8(d), a notable contribution to the ground movement is attributed to the system's main torsional frequency, identified at 3.8 Hz (as summarized in Table 1).

However, this torsional frequency is not observable in the superstructure's own vibration records (as previously mentioned and illustrated in Fig. 5), which is expected considering its low Modal Mass (MM) contribution of only 1 % (Table 1). The current study leverages realistic modeling and actual field records to clearly illustrate the relevance of flexibility in both the foundation and the superstructure (evidenced by the modal mass ratios presented in Table 1). This comprehensive approach complements existing studies found in the literature where SSI analysis often focused solely on the rigid body movement of the superstructure supported on soft soil [7].

The simplification to a 2-DOF representation facilitated the use of elementary equations for the dynamic identification of the system. Specifically, Eq. 3 [43] was used to calculate the two main lateral

Table 2
Soil and Superstructure properties.

	Actual Records	FE original, $v_s = 150$ m/s				FE altern., $v_s = 133$ m/s				2-DOF model		
			MM*				MM*			2 models / same foundation		
Frequency	f [Hz]	f [Hz]	x-dir	y-dir	error**	f [Hz]	x-dir	y-dir	error**	f [Hz]	MM*	error**
$f_{1\text{-}x}$	2.06	2.34	0.43	0.06	14 %	2.30	0.47	0.07	12 %	2.51	0.65	22 %
$f_{2\text{-}x}$	5.02	4.73	0.29	0.10	6 %	4.52	0.24	0.10	10 %	5.36	0.35	7 %
$f_{1\text{-}y}$	2.53	2.56	0.08	0.54	2 %	2.50	0.08	0.58	1 %	2.56	0.71	1 %
$f_{2\text{-}y}$	5.15	4.81	0.09	0.28	7 %	4.60	0.09	0.24	11 %	5.14	0.29	0 %
$f_{torsion}$	3.80	3.38	0.11	0.01	11 %	3.36	0.11	0.01	12 %		4-main freq. error =	8 %
$f_{1\text{-}x\text{-fixed}}$	2.77	2.54	0.53	0.08	8 %	2.54	0.53	0.08	8 %			
$f_{1\text{-}y\text{-fixed}}$	3.02	2.91	0.08	0.66	4 %	2.91	0.08	0.66	4 %			
				4-main freq. error =	7 %			4-main freq. error =	8 %			

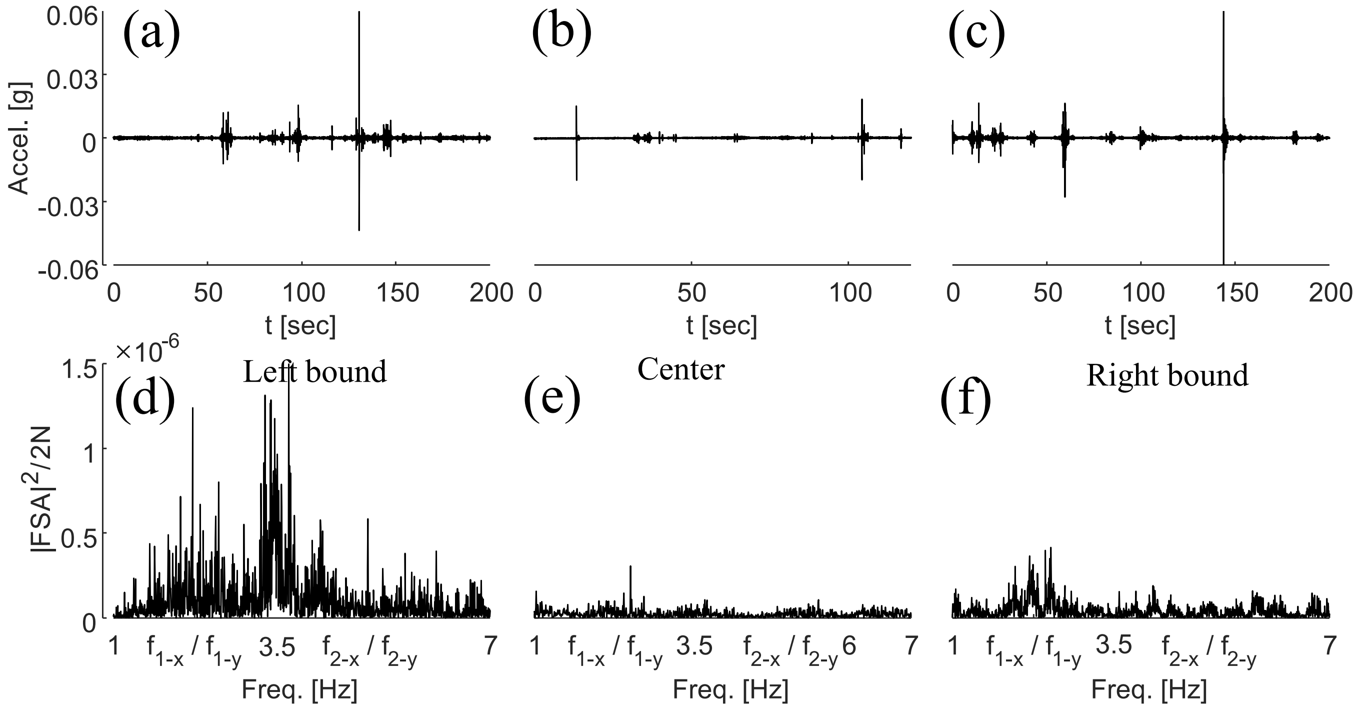

Fig. 8. Surrounding-ground vibrations along y-direction: (a), (b) and (c) are time-domain vibrations measured at surrounding foundation soil by the lower building side in Fig. 1(b); (d), (e) and (f) are power spectra of the respective time-domain records.

frequencies of the coupled building-foundation system along the y-direction. This equation incorporates the dimensionless ratios for mass ($\mu = m_b/m_f$) and frequency ($\eta = f_b/f_f$), whose numerical values are provided in Table 1. The measured fixed natural frequency ($f_{1\text{-y-fixed}}$), previously identified from spectral analysis (Fig. 6c), was also input into Eq. 3. The building mass (m_b), essential for the 2-DOF representation, was calculated using the combination of the fixed-base version of the full FE model (Fig. 9a) and the associated superstructure mass and stiffness matrices (Fig. 9b). To verify this SDOF representation of the superstructure, the fixed frequencies derived from the eigenvalue solution of the matrices in Fig. 9(b) were compared with the actual measured values listed in Table 1. By employing the experimentally identified SSI frequencies ($f_{1\text{-y}}$, $f_{2\text{-y}}$) from Fig. 5 and Table 1, Eq. 3 was solved for the frequency ratio (η), yielding a result with less than 1 % difference when compared to the two measured values.

The foundation stiffness (k_f) for this simplified 2-DOF model (Fig. 1d), analogous to the representation in the full FE model (Fig. 2), was then estimated via the inverted frequency parameter (η) using the relationship $k_f = 4\pi^{2*} m_{f*} f_f^2$, treating the foundation as a lumped-mass system. The foundation stiffness in the original model of Table 2 (total foundation stiffness of 2876 kN/mm) labeled as “original” was calculated based on a shear-wave velocity of $v_s = 150$ m/s corresponding to an upper limit according to micro-zonation studies and local explorations for the project. However, the foundation stiffness parameter determined empirically through the calibrated frequency ratio (η) was lower (2,491kN/mm in Table 2). This stiffness was used to back-calculate the effective shear wave velocity needed to match the empirical results, yielding $v_s = 133$ m/s—a value 10 % smaller than the initial estimate. The results derived from the updated FE model incorporating this revised soil stiffness are referred to as the "alternative" scenario in Tables 1 and 2. Comparison between the 'original' and 'alternative' model outcomes in Table 1 concluded that the predicted natural frequencies were relatively insensitive to the plausible variations in shear-wave velocities found. In both scenarios, the frequency estimates derived from the FE models remained within less than 10 % difference with respect to the actual field measurements. Based on this outcome, the numerical modeling was considered sufficiently calibrated for the purpose of this investigation.

$$f_{1,2}{}^2 = f_{fixed}{}^2\left[1 + (1+\mu)\eta^2 \mp \sqrt{\left[1 + (1+\mu)\eta^2\right]^2 - 4\eta^2}\right] \tag{3}$$

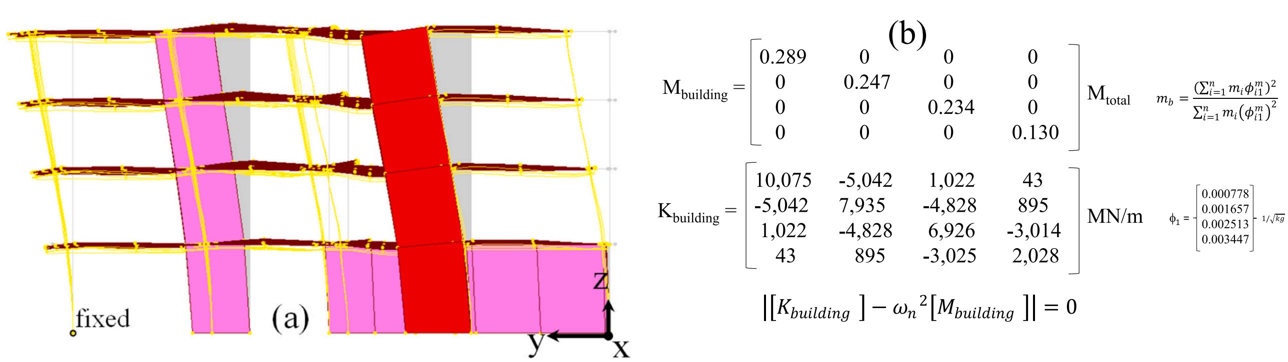

Fig. 9. Fixed-base version of the 3D FE Model and SDOF representation of building superstructure: (a) elevation-view of main y-direction mode shape; (b) mass and stiffness superstructure matrices derived from 3D model to calculate a one-DOF for the building superstructure.

6. Perceptible vibration and their source

This section presents qualitative and quantitative quantification of the perceived vibrations and the applied forces in the system, in order to confirm that SSI is the main factor in having perceivable vibrations. Figs. 10(a) and 10(b) illustrate the magnitude of measured vibrations near column 3 A on the fourth floor, the area where perceived vibrations were reported, according to the internationally recognized Reiher-Meister Chart for vibration control [45]. The effect of these vibrations is clearly more pronounced along the y-direction than the x-direction. This directional dominance can be attributed to several factors: The first y-direction frequency ($f_{1\text{-}y}$) constitutes the fundamental frequency of the entire system; The first fundamental frequencies in both the x and y directions contribute energy along the y-axis due to modal coupling; The presence of perimeter foundation walls creates a larger exposed area for the input of traffic-induced waves in the y-direction; Heavy traffic flow operates in close proximity to this highly exposed area. The level of perception indicated in these figures, when reporting x and y movements separately, falls into the "Barely noticeable to persons" category. However, considering the simultaneous occurrence of x and y movements, the resultant total vibration, estimated as the square root of the sum of the squares, would place the vibration category closer to "Easily noticeable to persons". The estimated natural frequency of the underlying soil strata ($f_{soil\text{-}stratum} = v_s/4H$) is between 1.6 Hz ($v_s = 133$ m/s) and 1.8 Hz ($v_s = 150$ m/s), using the micro-zonation study's lower-bound depth (H = 21 m).

For verification, if a shear-wave velocity of $v_s = 180$ m/s were selected—a value plausible for both Type D and Type E soil profiles specified in the local standard [2]—the estimated soil frequency would be 2.1 Hz. This frequency aligns closely with the building's natural frequencies (which range between 2.0 Hz and 2.5 Hz in both horizontal directions, as shown in Table 1). The proximity between the forcing frequency entering the foundation-building system (i.e., the soil's natural frequency, which is close to 2 Hz based on the characteristic period of the soil equal to 0.5 s, as indicated in the micro-zonation study [23]) and the building's SSI-frequency significantly determines the amplification effect of traffic waves transmitted through the soil media. The dynamic amplification factor from the ground level to the 4-th floor, calculated under harmonic excitation [46], is estimated to range between 1.4 and 2.1 across the three soil velocity scenarios examined (v_s of 150, 133, and 180 m/s). An auxiliary analysis focusing on the local vertical vibration of the slab in the critical area confirmed that

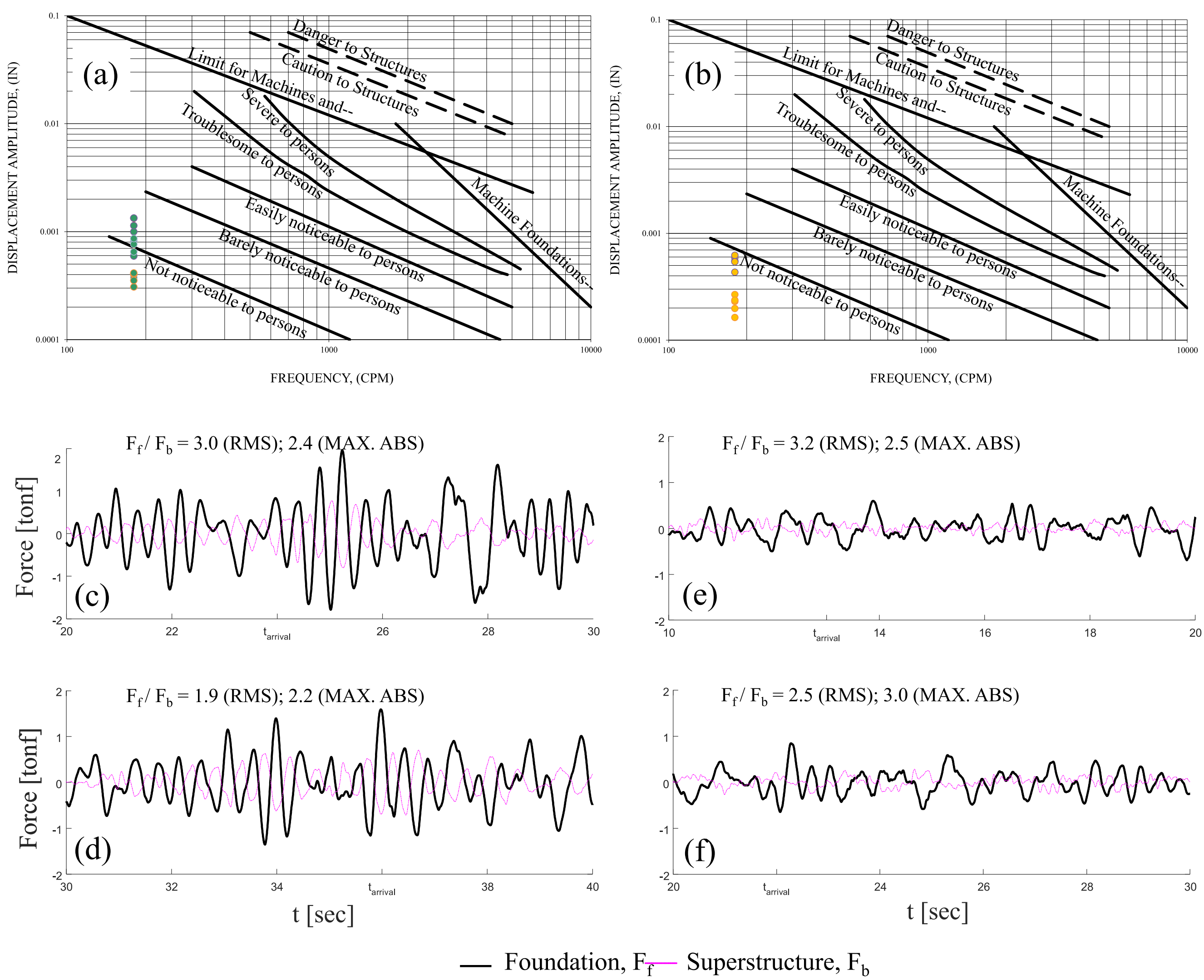

Fig. 10. Qualitative and quantitative estimates of vibrations perceived: (a) and (b) qualification of vibrations measured separately on y and x-direction respectively at 4-th floor, according to Reiher-Meister [28]; (c) and (d) estimated forces applied at foundation and superstructure for the measured vibrations along y-direction for two different passing-vehicle tests, based on a 2-DOF representation; (e) and (f) estimated forces applied at foundation and superstructure for the measured vibrations along x-direction for the same two passing-vehicle tests of (c) and (d), based on a 2-DOF representation.

movements unrelated to SSI are not the cause of the reported discomfort. The slab's natural vertical frequency of approximately 14 Hz (measured and verified with the 3D model), coupled with a measured acceleration of 0.2 millig, yielded a maximum displacement of only 0.3 microns. This displacement is far below the threshold for human perception, as defined by the lower region of Fig. 10(a). Furthermore, the risk of perceived vibrations due to human-walking effects was conclusively discarded using standardized formulations [47]. Therefore, it is concluded that vertical movement of the slab cannot cause noticeable vibrations to occupants in the reported critical building area.

To verify that traffic-induced waves at the foundation level are the primary source of the perceived vibrations, Eq. 2(b) was utilized to estimate the acting forces within the simplified 2-DOF system. Rather than assuming a predetermined forcing function, such as $F_o = \begin{Bmatrix} 1 \\ 0 \end{Bmatrix}$ (which represents force applied exclusively at the foundation), the right-hand side of the equilibrium equation was solved to account for forces applied simultaneously to both the foundation (F_f) and the superstructure (F_b). The unknown force variables, $F = \begin{Bmatrix} F_f(\Omega) \\ F_b(\Omega) \end{Bmatrix}$, were solved as a function of the excitation frequency, Ω. The displacement terms on the left-hand side of Eq. 2(b) were derived from the Fourier Transform of the accelerations measured at the foundation and the top floor during the controlled vehicle-passing tests. For the foundation DOF, these were calculated as as $X_f(\Omega) = -\ddot{X}_f(\Omega)/\Omega^2$.Once the forces were determined in the frequency domain, the corresponding force-time histories were generated using inverse Fourier transformations.

Figs. 10(c) through 10(f) present the estimated time-history forces applied to the foundation and superstructure during several controlled vehicle-passage tests. The instances of vehicle arrival ($t_{arrival}$) are indicated along the time axes. Because these estimates are derived from a simplified 2-DOF model, the magnitudes are likely overestimated due to the assumption of uniform floor displacement, which does not account for actual torsional contributions.

Furthermore, as the actual magnitude of loads arriving at the foundation diminishes rapidly with distance from the vehicle source [48], this analysis focuses on the relative comparison between superstructure and foundation force estimates to identify the primary source of excitation. The input force at the foundation (F_f) represents surface waves generated by traffic, while the superstructure input force (F_b) accounts for environmental effects such as wind or internal human activity. Figs. 10(c) and 10(d) provide results for the transverse (y-direction), while Figs. 10(e) and 10(f) correspond to the longitudinal (x-direction). Despite the presence of minor environmental noise during field testing, the estimated foundation forces exhibit a distinct spike coinciding with the vehicle arrival time. This demonstrate that foundation-level forces increase significantly as the vehicle passes directly in front of the building. It is also observed that forces are generated at other intervals, as superficial waves propagate to the structure faster than the vehicle itself. Consistent with the system's dynamic characteristics discussed previously, foundation forces in the y-direction are larger than those in the x-direction. In Figs. 10(c) through 9(e), the ratios of foundation-to-superstructure forces were quantified using:1) Root-mean-square (RMS) values and 2) Absolute maximum values. The results show that the estimated forces at the foundation are, on average, more than 2.5 times larger than the forces acting on the superstructure. This significant difference confirms that superficial waves generated by traffic are the dominant contributor to the perceived vibrations within the building. This procedure of force comparison at the two DOFs of the system to identify the energy-input source, confirms previous results: a) duality of fundamental frequencies observed in ambient vibrations in Fig. 5, b) presence of soil flexibility evidenced by TF of Fig. 6(c), c) nonlinear-elastic behavior of the system by illustrating the varying fundamental frequency illustrated in Fig. 6(a) and Fig. 7.

7. Conclusions

This study investigated a framed four-story reinforced concrete building with two underground levels founded in soft soil, where occupants reported perceptible vibrations at the left boundary of the top floor during service conditions. The method presented to identify SSI is based on establishing the coexistence of two fundamental frequencies, derived from flexibility of foundation engaged after certain trigger level, that still belongs to what could be called small amplitude range. In contrast to existing research where natural frequency changes due to permanent effects derived from expected large displacement scenarios like earthquakes, this study evidences coexistence of two fundamental frequencies in an elastic fashion. By utilizing ambient vibration records and controlled vehicle-passage tests in conjunction with 3D Finite Element (FE) and 2-DOF numerical models, the following conclusions are drawn. a) Mobilization of SSI: At extremely low overall drift ratios (0.0002 %), the building exhibits a flexible-foundation behavior rather than a fixed-base condition. This soil-structure interaction (SSI) causes an average reduction in natural frequency of 20 % relative to the fixed-base condition along the primary horizontal axis, which corresponds to a 40 % reduction in system stiffness. b) Vibration Source and Amplification: The vibrations perceived by users are the result of traffic-induced waves being amplified through the superstructure due to structural flexibility. Furthermore, the flexibility of the soil-pile system facilitates the conversion of these waves into effective foundation input forces (F_f). c) Factors Influencing Perceptibility: Even in buildings that fully comply with conventional strength-based structural standards, several factors increase susceptibility to SSI-induced vibrations. Foundation Type, shallow foundations or floating-pile systems are more prone to SSI mobilization, Frequency Proximity, resonance-like effects occur when the natural frequency of the soil strata ($f_{soil} = v_s / 4H$) aligns with the building-foundation frequency. The approximation T ~ N/10 typically provides an upper-bound frequency estimate for preliminary evaluations. Substructure Configuration, the presence of underground stories increases the energy input at the foundation level due to the large exposed surface area of perimeter retaining walls. Traffic Proximity, the presence of heavy vehicle traffic in the immediate vicinity of the structure.

The findings highlight the need for further investigation into incorporating flexibility and serviceability recommendations within building design standards. This would ensure occupant comfort by preventing excessive vibrations driven by soil-structure interaction. Opposite to current practice where SSI is focused mainly in seismic applications with an inelastic model, effect of SSI in service conditions may be complemented under the perspective of a nonlinear-elastic model. Future investigation of displacement-dependent flexibility of the foundation, would help in achieving a better understanding of the trigger levels of SSI in service conditions of a building. Although the method has been proved for the general condition of soft soil support, it may be restricted to rigid superstructures that do not allow for appearance of the fixed-base frequency.

Declaration of Competing Interest

The authors declare that they have no known competing financial interests or personal relationships that could have appeared to influence the work reported in this paper.

Acknowledgements

The author gratefully acknowledges INGETEC's commitment to the pursuit of knowledge and its application to practical industry solutions. This support was essential for the completion of this technical article.

References

[1] ACI (American Concrete Institute). Building Code Requirements from Structural Concrete and Commentary. ACI Committee 318. Michigan: Farmington Hills; 2002.
[2] AIS (Asociación Colombiana de Ingeniería Sísmica). Reglamento Colombiano de Construcción Sismo-Resistente. Bogotá. Colombia: D.C; 2012. April 2012.
[3] American Association of State Highway and Transportation Officials (AASHTO). LRFD Guide Specifications for the Design of Pedestrian Bridges. 2009.
[4] AISC (American Institute of Steel Construction) 2016. (Second Edition). Steel Design Guide 11, Vibrations of Steel-Framed Structural Systems due to Human Activity. Second Edition.
[5] ISO (International Organization for Standardization) 1997. Mechanical Vibration and Shock Evaluation of Human Exposure to whole-body Vibration. ISO 2631-1: 1997(E).
[6] Veletsos AS, Meek JW. Dynamic Behaviour of Building-Foundation Systems. Earthq Eng Struct Dyn 1974 1976;3:121. –38.
[7] Francois S, Masoumi L, Degrande G. The influence of dynamic soil–structure interaction on traffic induced vibrations in buildings. Soil Dyn Earthq Eng 2007;27 (2007):655–74.
[8] ISO (International Organization for Standardization). Bases for Design of Structures – Serviceability of Buildings and Walkways against Vibrations, 2007; 2007.
[9] Celebi M. "Comparison of damping in buildings under low-amplitude and strong motions. J Wind Eng Ind Aerodyn 1996;59(2-3):309–23.
[10] Novak M, Hifnawy L. Damping of Structures due to Soil-Structure Interaction. J Wind Eng Ind Aerodyn 1983;11(1-3):295–306.
[11] Stewart J, Seed R, Fenves G. SEISMIC SOIL-STRUCTURE INTERACTION IN BUILDINGS. II: EMPIRICAL FINDINGS. Journal of Geotechnical and Geoenvironmental Engineering. ASCE; 1999. ISSN 1090-0241/99/0001-0038–0048. Paper No. 16526.
[12] ASCE (American Society of Civil Engineers). Minimum Design Loads and Associated Criteria for Buildings and Other Structures. 2016.
[13] European Commission. Eurocode, Actions on Structures, 2002; 2002.
[14] AAHSTO (American Association of State Highway and Transportation Officials). AAHSTO LRFD Bridge Design Specifications. 2012.
[15] Mylonakis G, Gazetas. Seismic soil-structure interaction: beneficial or detrimental? J Earthq Eng 2000;4(2000):277–301. No. 3.
[16] Baban Lars A, Torsten W, Prada-Sarmiento L. "Soil-structure interaction: A state-of-the art review of modeling techniques and studies on seismic response of building structures. February 2023 Frontiers 2023. https://doi.org/10.3389/fbuil.2023.1120351.
[17] Stewart J, Seed R, Fenves G. SEISMIC SOIL-STRUCTURE INTERACTION IN BUILDINGS. I: ANALYTICAL METHODS. Journal of Geotechnical and Geoenvironmental Engineering. ASCE; 1999. ISSN 1090-0241/99/0001-0026–0037. Paper No. 16525.
[18] Cruz C, Miranda E. "Damping Ratios of the First Mode for the Seismic Analysis of Buildings". Journal of Structural Engineering, ASCE. ISSN; 2021. 0733-9445.
[19] Zhang X, Far H. "Seismic behaviour of high-rise frame-core tube structures considering dynamic soil–structure interaction". Bull Earthq Eng 2022. https://doi.org/10.1007/s10518-022-01398-9.
[20] Tahghighi1 H, Mohammadi2 A. "Numerical Evaluation of Soil–Structure Interaction Effects on the Seismic Performance and Vulnerability of Reinforced Concrete Buildings". International Journal of Geomechanics. ASCE; 2020. ISSN 1532-3641.
[21] Gonzalez JM, Barbat A, Vargas-Alzate Y, Rastellini F, Ramirez J, Escudero C, Pujades L. "Advanced nonlinear soil-structure interaction model for the seismic analysis of safety-related nuclear structures". –7488 Bull Earthq Eng 2024;22 (2024):7465. https://doi.org/10.1007/s10518-024-02055-z.
[22] De Sanctis L, Lovino M, Di Laora R, Aversa S. "Relevance of Dynamic Soil-Foundation-Structure Interaction for Pile-Supported Buildings". J Geotech Geoenviron Eng © ASCE 2020. ISSN 1090-0241.
[23] District of Bogotá 2010. District of Bogotá. 2010. Decree 523, "Seismic Micro-zonation of Bogota".
[24] IBC (International Building Code). 2021.
[25] USCS (Unified Soil Classification System).
[26] Adams DE. Health Monitoring of Structural Materials and Components. Methods with Applications. Wiley; 2010.
[27] Computers and Structures, I 2003. Berkeley, CA, Static and Dynamic Finite Element Analysis of Structures.
[28] Novak M. 1974. Dynamic Stiffness and Damping of Piles. Geotech J 1974;11:574.
[29] Das B. Principles of Foundation Engineering. Cengage Learning; 2023.
[30] Davis EH, Poulos HG. The use of elastic theory for settlement prediction under three-dimensional conditions. Geotechnique 1968;18(1):67–91. 1968.
[31] The MathWorks, I 2004. MATLAB, The Language of Technical Computing.
[32] Oppenheim AV, Schafer RW, Buck JR. Discrete-Time Signal Processing, 1999. Pearson Education; 1999.
[33] Proakis J. and Manokalis. Digital Signal Processing. Pearson; 2014.
[34] Consuegra F, Irfanoglu A. Variation of Small Amplitude Vibration Dynamic Properties with Displacement in Reinforced Concrete Structures. Exp Mech 2012. https://doi.org/10.1007/s11340-011-9590-0.
[35] Consuegra F, Fick D, Irfanoglu A. Using Nonlinear-Elastic Stiffness at Small Displacements to Identify Damage in a Full-Scale Reinforced Concrete Structure. Journal of Performance of Constructed Facilities. ASCE; 2024. ISSN 0887-3828.
[36] Clough RW, Penzien J. Berkeley, CA. Dynamics of structures: McGraw-Hill, New York, 1975. Computers and Structures Inc; 2014.
[37] Farrar C., Worden K., Todd M., Park G., Nichols J., Adams D., Bement M., Farinholt K. 2007. LA-14353-MS, November 2007. "Nonlinear System Identification for Damage Detection", Los Alamos National Laboratory, LA-14353-MS, November 2007.
[38] Wigner EP. "On the quantum correction for thermodynamic equilibrium. Phys Rev 1932;40:749–59.
[39] Bendat JS, Piersol AG. Random data: analysis and measurement procedures. New York: Wiley; 1986.
[40] Hao H, Ang TC, Shen J. Building vibration to traffic-induced ground motion. Build Environ 2001;36(2001):321–36.
[41] Xia H, Zhang N, Cao YM. Experimental Study of Train-induced Vibrations of Environments and Buildings. Journal of Sound and Vibrations, 280. Elsevier; 2005. p. 1017–29.
[42] Doyle JF. Wave propagation in structures: An FFT-based spectral analysis methodology. New York: Springer; 1989.
[43] Safak E. On Identification of Soil-Structure Interaction from recorded motions of Building. Earthquake Engineering, Tenth World Conference, 1992. Rottherdam: Balkema; 1992. ISBN 90 5410 060S.
[44] Safak E. Wave-Propagation Formulation of Seismic Response of Multistory Buldings. ASCE J Struct Eng 1999;125(4). April, 1999 SSN 0733-9445/99/0004-0426–0437.
[45] ACI (American Concrete Institute). Foundations for Dynamic Equipment. ACI Committee, 351; 2004. ACI 3513R-04.
[46] Chopra AK. Theory and Applications to Earthquake Engineering. NJ: Prentice-Hall, Inc; 1995.
[47] Allen D, Murray T. Design criterion for vibrations due to walking. Eng J Am Inst Steel Constr Fourth Quart 1993 1993.
[48] Auersch L. The excitation of ground vibration by rail traffic: Theory of Vehicle–Track–Soil interaction and measurements on high-speed lines. Journal of Sound and Vibration. Elsevier; 2005. https://doi.org/10.1016/j.jsv.2004.06.01.